Research Article

Wael Al-Kouz, Syed Zahir Hussain Shah, Basma Souayeh*, Zulqurnain Sabir, and Wahib Owhaib

A novel tetra hybrid bio-nanofluid model with stenosed artery

https://doi.org/10.1515/phys-2024-0091
received February 03, 2024; accepted September 25, 2024

Abstract: For treating and diagnosing cardiovascular diseases, the field of biomedical engineering is significant because it develops new ways and techniques. Stenosis is the narrowing of an artery, and it leads reduction in the flow rate of blood. This study investigates the blood flow mechanism in an artery using a mathematical model of Carreau nanofluid with four distinct nanoparticles. Tetra nanofluid model produces significant advancement in the simulation of blood flow through the stenosed arteries. The model is capable of predicting the pressure drop and velocity distribution for diagnosing and treating stenosis. The spectral relaxation approach is used to present the model's efficiency and effectiveness, which makes it a suitable method for solving the governing equations of this study. The findings of this study have important implications for the development of new treatments and diagnostic techniques for stenosis and other cardiovascular diseases.

Keywords: carreau fluid, tetra hybrid nanofluid, spectral relaxation approach, viscous dissipation, Joule heating, nonlinear thermal radiation

*** Corresponding author: Basma Souayeh,** Department of Physics, College of Science, King Faisal University, P. O. Box 400, Al-Ahsa, 31982, Saudi Arabia; Laboratory of Fluid Mechanics, Physics Department, University of Tunis El Manar, Tunis, 2092, Tunisia, e-mail: bsouayeh@kfu.edu.sa, basma.souayeh@gmail.com
Wael Al-Kouz: Department of Engineering and Industrial Professions, University of North Alabama, Florence, AL, 35630, United States of America, e-mail: walkouz@una.edu
Syed Zahir Hussain Shah: Department of Mathematics & Statistics, Hazara University, Manshera, 21300, Pakistan, e-mail: zahirkazmi5@yahoo.com
Zulqurnain Sabir: Department of Computer Science and Mathematics, Lebanese American University, Beirut, Lebanon, e-mail: zulqurnain.sabir@lau.edu.lb
Wahib Owhaib: Department of Mechanical and Maintenance Engineering, German Jordanian University, Amman 11180, Jordan, e-mail: wahib.owhaib@gju.edu.jo

1 Introduction

Stenosis is the abnormal position of the artery. In this case, the artery becomes narrow in the body, and it occurs in the spinal canal and blood vessels. This constriction in the way of the artery gives restricted blood flow and keeps nerves. This issue can be addressed by involving surgical interventions. Recent advancements in nanotechnology offer that this issue can be solved using the incorporation of nanoparticles in blood. Nanoparticles can be engineered to carry drugs or imaging agents, allowing for both treatment and real-time monitoring of the condition. Many scholars [1–3] performed the analysis regarding the blood vessels and arteries based on the fluidic models. Zhao *et al.* [4] made an exploration regarding the correlations between stenosis analysis and a connected microfluidic model of thrombosis. Akhtar *et al.* [5] delved into the non-Newtonian behavior of blood with consideration electro-osmotic effects and multiple stenoses. Das *et al.* [6] investigated transient Casson fluid flow in which they incorporated solute dispersion effects. Shahzad *et al.* [7] examined numerical results using a non-Newtonian Casson fluid model coupled with stenosis and elastic walls.

Magnetohydrodynamics (MHD) is study of fluids in the presence of magnetic fields. MHD becomes significant due to the conductive properties of blood and the potential presence of magnetic nanoparticles. When blood flows through arteries in the presence of magnetic nanoparticles then their interactions between magnetic field and electric currents in the blood can influence flow patterns. Furthermore, MHD has medical applications [8–13] like optimizing the delivery efficiency, targeted drug delivery, and distribution of therapeutic agents within the bloodstream. Al-Kouz *et al.* [14] investigated the thermal behavior of ternary hybrid nanofluid flow around the cylinder in a magnetized environment. In this study, they concluded that magnetic field has effects on heat transport. Al-Rashed *et al.* [15] explored vorticity–vector potential formalism on the open cavity filled by the aluminum oxide/water nanofluid. The cavity is heated up by the central isothermal block and the results of mixed convection and entropy generation. Bakthavatchalam *et al.* [16]

published their review studies about nanofluid and ionanofluid for heat transfer enhancement, they have reviewed current and future perspectives. Shulepova *et al.* [17] delve into the mathematical modeling of convective energy transport in an enclosure with moving upper adiabatic walls and vertical isothermal walls under the impacts of alumina–water nanoliquid and complicated fins within the cavity. Selimfendigil and Öztop [18] made their study of the thermal and phase change process in a branching T-channel under an active magnetic field and two rotating inner cylinders. In another study, Selimfendigil *et al.* [19] investigated the optimization of a bifurcating channel cooling system for a double-inclined conductive panel system under an inclined magnetic field. Selimfendigil and Öztop [20] performed a numerical analysis on multijet impingement heat transfer under the combined effects of encapsulated-PCM and inclined magnetic field during nanoliquid convection. There are latest studies [21–26] related to MHD flow with different facts like activation energy and inclined magnetic dipole, bio-nanofluid model in expanding/contracting cylinder, biological interactions of cross fluid with inclined MHD, buoyancy force and melting heat process.

Heat transport in bio-nanofluids with nanoparticles is crucial for practical applications and research avenues. Bio-nanofluids offer potential in biomedical engineering like hyperthermia therapy, drug delivery, and diagnostic imaging. Efficient heat transport within these fluids plays a pivotal role in targeted drug delivery and precise control of temperature distribution within the bio-nanofluid can enhance drug release kinetics and therapeutic efficacy. Therefore, investigating heat transport mechanisms in bio-nanofluids with nanoparticles advances innovation in biomedical technologies with significant implications for healthcare. It is evidence from old literature [27–32] that heat transport can be enhanced by including nanoparticles in the base fluid. The investigation of blood flow characteristics using various nanofluid models presents a rich area of research with diverse applications in biomedical engineering. Algehyne *et al.* [33] gave their numerical study, and it is proved that heat transfer is enhanced in blood flow using hybrid Ag–TiO_2 nanoparticles. In this study electrical field is also considered and cylindrical w-shape stenosis artery was under consideration. Darvesh *et al.* [34] conducted numerical and mathematical analysis related to bio-nanofluid over a nonlinear tapering artery. In this study, authors discussed the stenosis conditions with the cross nanofluid model. Sharma *et al.* [9] concluded that heat transfer is optimized in blood flow. In this study, hall effect and variable viscosity facts are also considered. Khan *et al.* [35] made heat transport analysis with entropy-optimized generation with nanoparticles over disks geometry. These studies contribute to advancing heat transport in blood nanofluid systems.

1.1 Applications of heat transfer in blood flow

Rote of heat transfer is crucial in various industries and engineering areas because it facilitates processes like energy production, food processing and manufacturing. However, its significance extends even further, particularly in medical science and healthcare, like the removal of stenosed arteries. Controlled heat can effectively target and restore proper blood flow, dissolve blockages within blood vessels, and prevent severe health complications like heart attacks or strokes.

1.2 Motivation

The motivation to study a novel tetra hybrid bio-nanofluid model with a stenosed artery stems from the pressing need to optimize the dynamics of blood flow in vascular conditions. Stenosed arteries are abnormally narrow pose, and it has a risk of cardiovascular diseases.

1.3 Novelty

This study employs a novel tetra hybrid bio-nanofluid model to investigate blood flow dynamics in stenosed arteries. In this study, mathematical modeling of Carreau nanofluid with four distinct nanoparticles is considered.

2 Creation of physical model

It is supposed that blood is flowing in a horizontal artery whose length is $\frac{L_0}{2}$. Blood is assumed to flow through as x-axis and radial axis r. Inclined magnetic field is imposed on the blood flow with an angle ω based on the horizontal artery. To investigate the blood's temperature, the facts of non-uniform heat sink/source, joule heating, and thermal radiation are included. Prototype shows the extension of nanofluid determined by Tiwari and Das, which has been included in blood to investigate the impact of four kinds of nanoparticles based on the blood flow passing through the artery. The radius of the artery is denoted by $R^*(x)$ and λ is the maximum height. The area of stenosed is given by $R^*(x) = R_0 - \frac{\lambda}{2}\left(1 + \cos\left(\frac{4\pi x}{L_0}\right)\right)$ where $x \in \left(\frac{-L_0}{4}, \frac{L_0}{4}\right) = R_0$. Its mean value of x will be between $\left(\frac{-L_0}{4}, \frac{L_0}{4}\right)$, and we said

it R_0. So, now $R^*(x) = R = R_0 - \frac{\lambda}{2}\left(1 + \cos\left(\frac{4\pi R_0}{L_o}\right)\right)$. Figure 1 is placed for physical configuration of flow. Furthermore, the thermophysical characteristics of nanoparticle are given in Table 1.

Based on physical assumptions, the equation of continuity, momentum, and temperature are given as:

$$\frac{\partial(ru)}{\partial x} + \frac{\partial(rv)}{\partial r} = 0, \tag{1}$$

$$\rho_{\text{tethnf}}\left(u\frac{\partial u}{\partial x} + v\frac{\partial v}{\partial r}\right) = \frac{\mu_{\text{tethnf}}}{r}\frac{\partial}{\partial r}\left[\frac{\partial u}{\partial r}\left(1 + \left(\Gamma\frac{\partial u}{\partial r}\right)^2\right)^{\frac{(n-1)}{2}}\right] - \sigma_{\text{tethnf}}B_o{}^2\sin^2(\varpi)u, \tag{2}$$

$$(\rho C_p)_{\text{tethnf}}\left(u\frac{\partial T}{\partial x} + v\frac{\partial T}{\partial x}\right) = \frac{k_{\text{tethnf}}}{r}\frac{\partial}{\partial r}\left(r\frac{\partial T}{\partial x}\right) + \frac{\partial}{\partial r}\left(\frac{16\sigma^{**}T_\infty{}^3\partial T}{3\kappa^{**}\partial r}\right) + \mu_{\text{tethnf}}\left(\frac{\partial u}{\partial x}\right)^2 + \sigma_{\text{tethnf}}B_0^2(u)^2 + Q^*(T - T_\infty). \tag{3}$$

Attached BCs are,

$$\begin{Bmatrix} r = R: \ u = u_o, \ v = 0, \ T = T_w, \\ r \to \infty: \ u \to 0, \ T \to T_\infty. \end{Bmatrix}. \tag{4}$$

Physical relation in mathematical forms.

$$\mu_{\text{tethnf}} = \mu_f[(1-\phi_1)^{2.5}(1-\phi_2)^{2.5}(1-\phi_3)^{2.5}(1-\phi_4)^{2.5}]^{-1}, \tag{5}$$

$$\rho_{\text{tethnf}} = \begin{bmatrix} (1-\phi_1)\left\{(1-\phi_2)(1-\phi_3)\begin{bmatrix}(1-\phi_4)\phi_f \\ +\rho_4\phi_4\end{bmatrix} + \rho_3\phi_3\right. \\ \left. + \rho_2\phi_2\right\} + \begin{bmatrix}(1-\phi_4)\phi_f \\ +\rho_4\phi_4\end{bmatrix} + \rho_3\phi_3 + \rho_1\phi_1 \end{bmatrix}, \tag{6}$$

Table 1: Thermophysical characteristics [36–38] of TiO_2, Au, Al_2O_3 & Ag on blood

Properties	Blood	Gold (Au)	TiO_2	Silver (Ag)	Al_2O_3
ρ	1,050	19,300	4,250	10,500	3,970
C_p	3,617	129	690	235	765
K	0.52	310	8.953	429	40
σ	0.667	4.1×10^6	2.4×10^6	6.3×10^7	3.5×10^7

$$(\rho C_p)_{\text{tethnf}} = \begin{bmatrix} (1-\phi_1)\left\{\begin{matrix}(1-\phi_2)(1-\phi_3) \\ [(1-\phi_4)(\rho C_p)_f + (\rho C_p)_{S_4}\phi_4]\end{matrix}\right\} \\ + (\rho C_p)_{S_4}\phi_3 + (\rho C_p)_{S_2}\phi_2 + (\rho C_p)_{S_1}\phi_1 \end{bmatrix}, \tag{7}$$

$$\begin{aligned} \frac{k_{\text{tethnf}}}{k_{\text{hnf}}} &= \frac{k_1 + 2k_{\text{nf}} - 2\phi_1(k_{\text{nf}} - k_1)}{k_1 + 2k_{\text{nf}} + \phi_1(k_{\text{nf}} - k_1)}, \\ \frac{k_{\text{tethnf}}}{k_{\text{hnf}}} &= \frac{k_2 + 2k_{\text{nf}} - 2\phi_2(k_{\text{nf}} - k_2)}{k_2 + 2k_{\text{nf}} + \phi_2(k_{\text{nf}} - k_2)}, \end{aligned} \tag{8}$$

$$\begin{aligned} \frac{k_{\text{tethnf}}}{k_{\text{hnf}}} &= \frac{k_3 + 2k_{\text{nf}} - 2\phi_3(k_{\text{nf}} - k_3)}{k_3 + 2k_{\text{nf}} + \phi_3(k_{\text{nf}} - k_3)}, \\ \frac{k_{\text{tethnf}}}{k_{\text{hnf}}} &= \frac{k_4 + 2k_{\text{nf}} - 2\phi_4(k_{\text{nf}} - k_4)}{k_4 + 2k_{\text{nf}} + \phi_4(k_{\text{nf}} - k_4)}, \end{aligned} \tag{9}$$

$$\begin{Bmatrix} \frac{\sigma_{\text{tethnf}}}{\sigma_{\text{hnf}}} = \frac{(1+2\phi_4)\sigma_4 + (1-2\phi_4)\sigma_{\text{tethnf}}}{(1-\phi_4)\sigma_4 + (1+\phi_4)\sigma_{\text{tethnf}}}, \\ \frac{\sigma_{\text{tethnf}}}{\sigma_{\text{hnf}}} = \frac{(1+2\phi_3)\sigma_3 + (1-2\phi_3)\sigma_{\text{hnf}}}{(1-\phi_3)\sigma_3 + (1+\phi_3)\sigma_{\text{hnf}}}, \\ \frac{\sigma_{\text{hnf}}}{\sigma_{\text{nf}}} = \frac{(1+2\phi_2)\sigma_2 + (1-2\phi_2)\sigma_{\text{nf}}}{(1-\phi_2)\sigma_2 + (1+\phi_2)\sigma_{\text{nf}}}, \\ \frac{\sigma_{\text{nf}}}{\sigma_f} = \frac{(1+2\phi_1)\sigma_1 + (1-2\phi_1)\sigma_f}{(1-\phi_1)\sigma_1 + (1+\phi_1)\sigma_f}, \end{Bmatrix}. \tag{10}$$

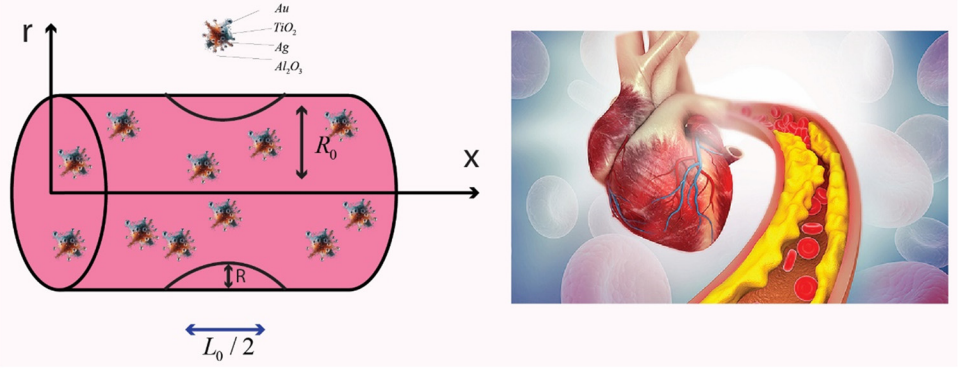

Figure 1: Geometry of blood flow *via* arteries.

3 Solution procedure

Transformations are as follows:

$$\eta = \sqrt{\frac{(r^2 - R^2)^2 u_0}{4R^2 \upsilon L_0}},\ u = \frac{u_0 x}{L_0} f'(\eta),$$
$$v = \sqrt{\frac{R^2 u_0 v}{r^2 L_0}} f(\eta),\ \theta(\eta) = \frac{T - T_\infty}{T_w - T_\infty}. \tag{11}$$

Using required material in governing equations, we get

$$\begin{aligned}&(1 + 2\gamma\eta)(1 + n(\mathrm{We}(f'')^2))(1 + (\mathrm{We}(f'')^2))^{\frac{n-3}{2}} f''' \\ &\quad + 2\gamma f'' A^* B^* \left[1 + \left(1 - \frac{n}{2}\right)(\mathrm{We} f'')^2\right] \\ &+ A^* B^* [f f'' + (f')^2 - C^* M f''] = 0,\end{aligned} \tag{12}$$

$$\begin{aligned}&D^*(1 + R_d)(1 + 2\gamma\eta)\theta'' + 2\gamma\theta'(1 + (\theta_w - 1)\theta)^2, \\ &\quad + \{3(\theta')^2(\theta_w - 1)(1 + 2\gamma\eta) + 2\gamma\theta'(1 + (\theta_w - 1)\theta) \\ &\quad + \theta''(1 + 2\gamma\eta)(1 + (\theta_w - 1)\theta)\}, \\ &\quad + P_r E^* f\theta' + C^* M p_r E_c (f')^2 + \frac{(1 + 2\gamma\eta)E^*}{A^*}(f'')^2 + Q\theta = 0,\end{aligned} \tag{13}$$

Corresponding BCs,

$$\begin{Bmatrix}\eta = 0 : f(\eta) = 0, f'(\eta) = 1,\ \theta = 1, \\ \eta \to \infty :\ f(\eta) \to 0,\ \theta(\eta) \to 0.\end{Bmatrix}. \tag{14}$$

Local surface friction and Nusselt number are:

$$Cf\ \mathrm{Re}_x^{\frac{1}{2}} = A^* \left(\{1 + (\mathrm{We} f'')^2\}^{\frac{n-1}{2}} f''\right), \tag{15}$$

$$\mathrm{Nu}_x\ \mathrm{Re}_x^{-\frac{1}{2}} = -\{D^* + R_d[1 + (\theta_w - 1)\theta]^3\}\theta', \tag{16}$$

$$\begin{aligned}&A^* = \frac{\mu_{\mathrm{tethnf}}}{\mu_f},\ B^* = \frac{\rho_{\mathrm{tethnf}}}{\rho_f},\ C^* = \frac{\sigma_{\mathrm{tethnf}}}{k_f}, \\ &D^* = \frac{k_{\mathrm{tethnf}}}{k_{\tilde{f}}},\ D^* = \frac{(\rho C_p)_{\mathrm{tethnf}}}{(\rho C_p)_f}.\end{aligned} \tag{17}$$

4 Numerical scheme

There are several numerical techniques like bvp4c, Keller box, neural networks, and Lobatto IIIA, but in this study, the spectral relaxation method (SRM) has been utilized to solve nonlinear systems of ordinary differential equation (ODEs) (13) and (14) involved in this study.

4.1 SRM

The solution of the obtained differential model is presented by using the SRM. In this context, the method involves approximating the solution based on the ODE as a linear combination of basic functions, and then finding the coefficients of this linear combination based on the optimization problem with the formulation of a semidefinite program. The general idea of the SRM to solve the ODEs is to convert into a set of algebraic equations by discretizing the independent variable (usually time) to approximate the solution based on the basis functions. These basis functions are typically chosen to be orthogonal functions, such as Legendre polynomials or Chebyshev polynomials. Once the ODE has been discretized and approximated using basis functions, the resulting system of algebraic equations is then solved using an optimization method based on semidefinite programming. The optimization problem involves minimizing the residual error between the approximated solution and the exact solution of the ODE subject to a set of constraints, which can be expressed as linear or semidefinite constraints.

4.2 Advantages of SRM

There are several advantages of SRM to get the solutions of the differential system. Some of them are given as:

High accuracy: SRM can provide high-accuracy solutions of the model based on the differential model with a complex or non-analytic nature. The SRM has a spectral approximation of the solution and can be used to capture the high-frequency components of the solution.

Fast convergence: SRM can converge to the solution of an ODE faster than some other numerical methods, such as finite difference or finite element methods. SRM involves the solutions of a convex optimization problem, which can be faster to solve than non-convex problems.

Parallelizability: SRM can be easily parallelized, which makes it suitable for solving the large-scale differential models on high-performance computing platforms. The optimization subproblem can be solved independently, and the final solution is obtained by combining the outcomes of each subproblem.

Robustness: SRM is considered one of the robust methods that handle different forms of the differential models with stiff and non-stiff nature.

Versatility: SRM can also be applied to solve the differential model by using different types of boundary conditions, some of which are Dirichlet, Neumann, and mixed boundary conditions. It can also be extended to solve partial differential equations by using spectral approximations in both time and space.

4.3 Comparison of Bvp4c and SRM

Bvp4c is a robust numerical technique, and it solves the BVP efficiently. Adaptive mesh refinement and iterative algorithms are adopted in this scheme to approximate the solution to high accuracy. It is suitable for problems with nonlinearities with boundary conditions and it offers reliable convergence and stability. In comparing the two methods, Bvp4c excels in handling nonlinear boundary value problems and offers greater flexibility in dealing with various types of boundary conditions. It is well-suited for problems where accuracy and robustness are paramount. Conversely, the SRM is highly efficient for problems with smooth solutions and periodic boundary conditions, providing fast convergence and high accuracy.

4.4 Comparison of Keller Box and SRM

Keller Box method (KBM) and the SRM for solving ODEs involve contrasting their distinct approaches and applicability in solving boundary value problems. The Keller Box method employs shooting techniques to solve boundary value problems iteratively. SRM utilizes spectral approximations, often employing Fourier or Chebyshev basis functions, to discretize the differential equations. KBM discretizes the problem domain and solves the resulting system of initial value problems using numerical integration techniques. SRM transforms the differential equations into algebraic equations using spectral methods and solves the resulting system iteratively. KBM is suitable for problems with singularities or discontinuities in the solution.

4.5 Mathematical procedure for SRM

Step 1: For the iteration, the values $f = f_{r+1},\ \theta = \theta_{r+1}$, in Eqs. (12) and (13) are fixed as

$$\begin{aligned}&(1+2\gamma\eta)(1+n(\mathrm{We}(f''_{r+1})^2))(1+(\mathrm{We}(f''_{r+1})^2))^{\frac{n-3}{2}}\\&\quad f'''_{r+1}+2\gamma f''_{r+1}A^*B^*\left[1+\left(1-\frac{n}{2}\right)(\mathrm{We}f''_{r+1})^2\right]\\&\quad +A^*B^*[f_{r+1}f''_{r+1}+(f'_{r+1})^2-C^*Mf''_{r+1}]=0,\end{aligned}\tag{18}$$

$$\begin{aligned}&D^*(1+R_\mathrm{d})(1+2\gamma\eta)\theta''_{r+1}+2\gamma\theta'_{r+1}(1+(\theta_w-1)\theta_{r+1})^2\\&\quad +\{3(\theta'_{r+1})^2(\theta_w-1)(1+2\gamma\eta)\\&\quad +2\gamma\theta'_{r+1}(1+(\theta_w-1)\theta_{r+1})+\theta''_{r+1}(1+2\gamma\eta)(1\\&\quad +(\theta_w-1)\theta_{r+1})\}+P_rE^*f_{r+1}\theta'_{r+1}+C^*Mp_rE_\mathrm{c}(f'_{r+1})^2\\&\quad +\frac{(1+2\gamma\eta)E^*}{A^*}(f''_{r+1})^2+Q\theta_{r+1}=0.\end{aligned}\tag{19}$$

Parallel BCs for ODEs are given as:

$$\begin{Bmatrix}\eta=0: f_{r+1}(\eta)=0, f'_{r+1}(\eta)=1,\ \theta_{r+1}=1,\\ \eta\to\infty:\ f'_{r+1}(\eta)\to 0,\ \theta_{r+1}(\eta)\to 0.\end{Bmatrix}.\tag{20}$$

Step 2: Further iterations are performed by fixing $f'_{r+1}=\lambda,\ f_{r+1}(0)=0$,

$$\begin{aligned}&(1+2\gamma\eta)(1+n(\mathrm{We}(\lambda'_{r+1})^2))(1+(\mathrm{We}(\lambda'_{r+1})^2))^{\frac{n-3}{2}}\lambda''_{r+1}\\&\quad +2\gamma\lambda'_{r+1}A^*B^*\left[1+\left(1-\frac{n}{2}\right)(\mathrm{We}\lambda'_{r+1})^2\right]\\&\quad +A^*B^*[f_{r+1}\lambda'_{r+1}+(\lambda_{r+1})^2-C^*M\lambda'_{r+1}]=0,\end{aligned}\tag{21}$$

$$\begin{aligned}&D^*(1+R_\mathrm{d})(1+2\gamma\eta)\theta''_{r+1}+2\gamma\theta'_{r+1}(1+(\theta_\mathrm{w}-1)\theta_{r+1})^2\\&\quad +\{3(\theta'_{r+1})^2(\theta_\mathrm{w}-1)(1+2\gamma\eta)\\&\quad +2\gamma\theta'_{r+1}(1+(\theta_\mathrm{w}-1)\theta_{r+1})+\theta''_{r+1}(1+2\gamma\eta)(1\\&\quad +(\theta_\mathrm{w}-1)\theta_{r+1})\}+P_rE^*f_{r+1}\theta'_{r+1}+C^*Mp_rE_\mathrm{c}(\lambda_{r+1})^2\\&\quad +\frac{(1+2\gamma\eta)E^*}{A^*}(\lambda'_{r+1})^2+Q\theta_{r+1}=0.\end{aligned}\tag{22}$$

Parallel BCs for ODEs are given as:

$$\begin{Bmatrix}\eta=0: f_{r+1}(\eta)=0, \lambda_{r+1}(\eta)=1,\ \theta_{r+1}=1,\\ \eta\to\infty:\ \lambda_{r+1}(\eta)\to 0\ ,\ \theta_{r+1}(\eta)\to 0\ .\end{Bmatrix}.\tag{23}$$

Step 3:

$$\begin{Bmatrix}A_1\lambda_{r+1}=B_1,\ A_2\theta_{r+1}=B_2,\\ A=D^1,\ B=\mathrm{Sr}\\ A_2=D^2+\mathrm{Diag}(\theta_{r+1})D\end{Bmatrix},\tag{24}$$

$$\begin{aligned}B_2=&\frac{-1}{(1+2\gamma\eta)(1+n(\mathrm{We}(\lambda'_{r+1})^2))(1+(\mathrm{We}(\lambda'_{r+1})^2))^{\frac{n-3}{2}}}\\&\times\begin{bmatrix}\lambda''_{r+1}+2\gamma\lambda'_{r+1}A^*B^*\left[1+\left(1-\frac{n}{2}\right)(\mathrm{We}\lambda'_{r+1})^2\right]\\ +A^*B^*[f_{r+1}\lambda'_{r+1}+(\lambda_{r+1})^2-C^*M\lambda'_{r+1}]\end{bmatrix},\end{aligned}\tag{25}$$

$$\begin{aligned}A_3=&\mathrm{diag}\Bigg((1+2\gamma\eta)(1\\&+n(\mathrm{We}(\lambda'_{r+1})^2))(1+(\mathrm{We}(\lambda'_{r+1})^2))^{\frac{n-3}{2}}\Bigg)D^2\\&+\mathrm{diag}\left(\left[1+\left(1-\frac{n}{2}\right)(\mathrm{We}\lambda'_{r+1})^2\right]\right)D+\mathrm{diag}(\alpha)I,\end{aligned}\tag{26}$$

$$\begin{aligned}B_3=&\frac{1}{D^*(1+R_\mathrm{d})(1+2\gamma\eta)}\\&\times\begin{bmatrix}3(\theta'_{r+1})^2(\theta_\mathrm{w}-1)(1+2\gamma\eta)\\ +2\gamma\theta'_{r+1}(1+(\theta_w-1)\theta_{r+1})+\theta''_{r+1}(1\\ +2\gamma\eta)(1+(\theta_w-1)\theta_{r+1})+P_rE^*f_{r+1}\theta'_{r+1}\\ +C^*Mp_rE_\mathrm{c}(\lambda_{r+1})^2+\frac{(1+2\gamma\eta)E^*}{A^*}(\lambda'_{r+1})^2\\ +Q\theta_{r+1}=0.\end{bmatrix},\end{aligned}\tag{27}$$

$$A_4 = (1 + 2\gamma\eta)(1 + \theta_{r+1}\varepsilon)D^2 + \text{diag}([-3(\theta'_{r+1})^2(\theta_w - 1)(1 + 2\gamma\eta) + \theta''_{r+1}(1 + 2\gamma\eta)(1 + (\theta_w - 1)\theta_{r+1})])D\}. \quad (28)$$

5 Validity

The study presents a valid and valuable contribution to the existing literature in the field of biomedical engineering. This study builds upon previous research, introducing a new model that incorporates the viscosity of cross fluid and the effect of nanoparticles on blood flow, and using the spectral relaxation approach to solve the complex differential equations. The study's results are consistent with previous research and offer new insights into the effects of stenosis on blood flow. Table 2 shows the numerical technique that is found smooth agreement with existing literature, while Figure 2 is the respective statical matching of Table 2.

6 Obtained results and debate on physical output

This article relates the study of blood flow through narrow or constricted arteries with a mathematical model of tetra hybrid cross nanofluid. This study proposes a new model for analyzing such fluid flow, which considers the properties of nanofluids and the viscosity of cross-fluids. The results of the study are likely to provide insight into the behavior of blood flow in stenosed arteries, which could ultimately lead to the development of new treatments or interventions for cardiovascular diseases.

This segment brings detailed debate on the physical behavior of the tetra hybrid nanofluid model with a viscosity of the cross fluid in blood passing through the Stenosed Artery. The numerical outcomes are fetched with the help of a fast convergent spectral relaxation technique, as the cross fluid model is capable of investigating the fluid in shear thinning and shear thickening regions. Variation of cross fluid index n gives two regions for different values. If numerical values of $n \in (0, 0.5)$, then it goes in the category of shear thinning, and if numerical values of $n \in (1, \infty)$, then it will give behavior of shear thickening region as well as with the comparison of Bi-Hybrid/Tri-Hybrid/Tetra-Hybrid nanofluid. Output and influence of all physical parameters with the classification of shear thinning and shear thickening are plotted through figures. The following numerical ranges are utilized in this attempt for graphing. Table 3 shows the description of the physical parameters with symbol and their ranges in the interval.

Table 2: Agreement shows of current study with old literature

Γ	Φ	Sarwar and Hussain [39]	Present
0.10	0.01	0.93	0.9476666
0.12	0.01	0.92	0.936754
0.14	0.01	0.91	0.957665
0.10	0.05	1.32	1.3343212

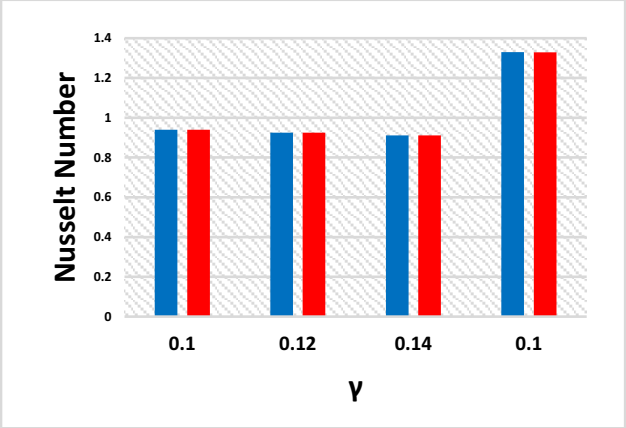

Figure 2: Statistical representation of Sarwar and Hussain [39] (blue color) compared to our present study (red color).

Table 3: Name of physical parameters with symbol and ranges in interval form

Name of physical parameter	Symbol and range of physical parameter in interval form
Thermal radiation	$R_d \in [0.8, 1.9]$,
Prandtl number	$\text{Pr} \in [18,21]$,
Temperature difference parameter	$\theta_w \in [0.5, 2.5]$
Eckert number	$E_c \in [0.1, 2.1]$
Curvature parameter	$\gamma \in [0.3, 2.5]$
Magnetic parameter	$M \in [0.1,5.1]$
Weissenberg number	$\text{We} \in [0.1, 4]$
Cross fluid index parameter	$n \in [0, 1]$ and $n \in (1, \infty)$
Heat sink/source parameter	$Q \in [0.5,\ 2]$
Inclined magnetic field angle	$\omega = 30^\circ,\ 45^\circ,\ 60^\circ,\ 90^\circ$

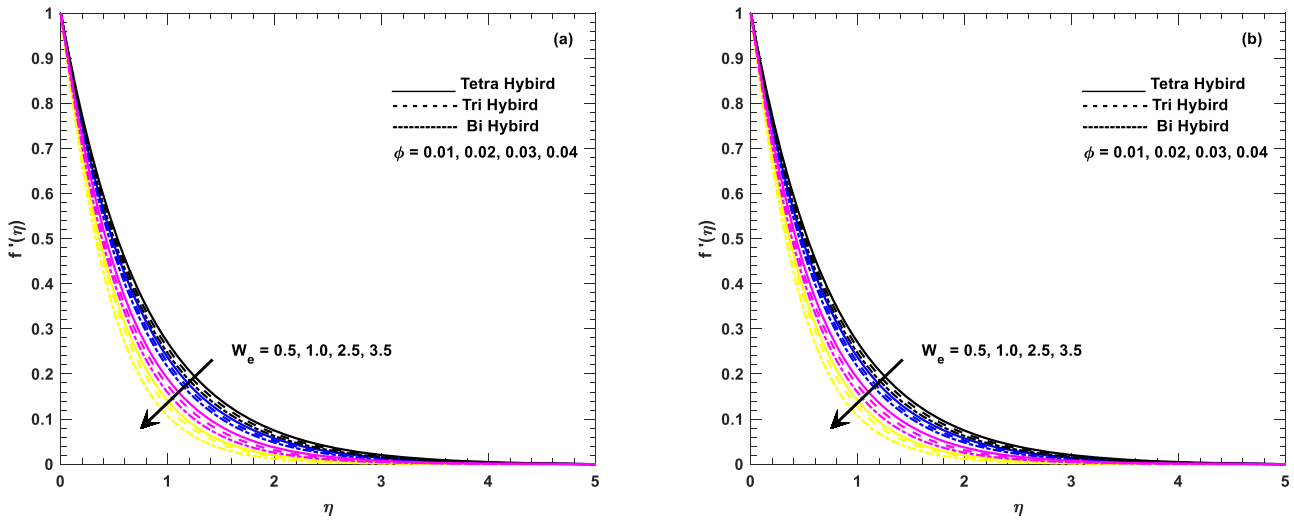

Figure 3: (a) and (b) Numerical assessment of We with speed of tetra hybrid cross nanofluid (blood) classifying shear thinning/thickening flow.

6.1 Numerical consequences of influential physical parameters attached to the velocity and temperature field of blood

The numerical result of We on the result of tetra hybrid cross nanofluid (blood) is presented in Figure 3(a) and (b). Greater numerical inputs in We give the lower speed of blood in both cases of shear thinning/thickening flow due to time relaxation constant involvement in the mathematical form of Weissenberg number. Low speed in blood cause several problems like reduced delivery of oxygen and nutrients, increased risk of blood clots, impaired waste removal, reduced immune response, poor healing, *etc.* Figure 4(a) and (b) is a pictorial representation of blood flow with numerical assessment of inclined angle ω. From the figure, it is clear that increasing the numerical value of the inclined angle reduces the velocity of bold. When the inclined angle increases, the strength of the magnetic field becomes perpendicular and a strong Lorenz force is generated, and this Lorentz force causes reduction in the velocity of the blood. It is also noted that Lorentz force may cause the blood to move in a circular or spiral pattern around the vessel, rather than in a straight line due to this linear velocity decreases. Figure 5 establishes the fact of numerical assessment of n with the speed of tetra hybrid cross nanofluid (blood). Greater value of cross fluid index converts the fluid in shear thickening. Due to the thickening situation of blood, its velocity goes down. Thick blood creates a lot of problems in the body. A disease due to thick blood is known as hypercoagulability. Thick blood

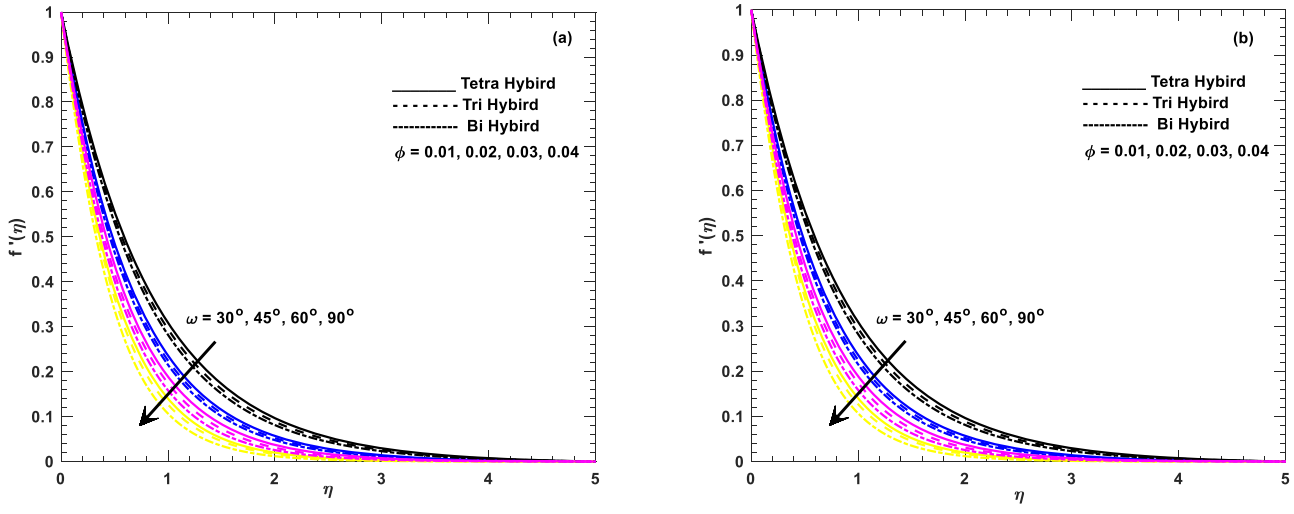

Figure 4: (a) and (b) Numerical assessment of ω with speed of tetra hybrid cross nanofluid (blood) classifying shear thinning/thickening flow.

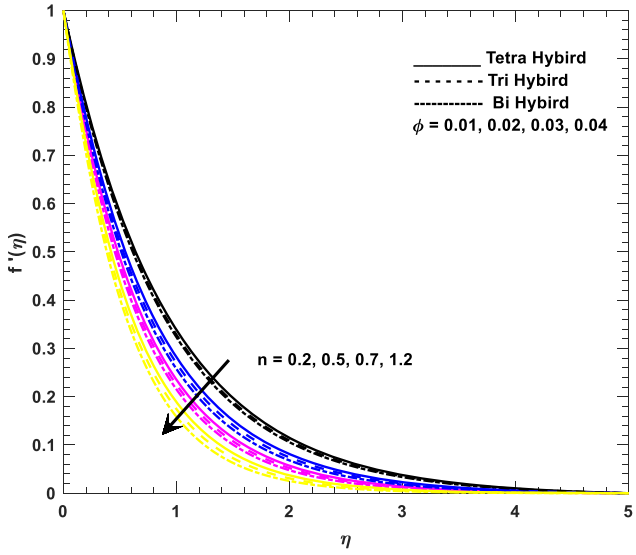

Figure 5: Numerical assessment of n with speed of tetra hybrid cross nanofluid (blood).

flows slowly in arteries and makes other problems like blood clots, increased risk of cardiovascular disease, and increased risk of deep vein thrombosis. Figure 6(a) and (b) depicts the numerical assessment of M with the speed of tetra hybrid cross nanofluid (blood) classifying shear thinning/thickening flow. Both cases show that a greater numerical value of M gives lower velocity because of Lorentz force. Figure 7(a) and (b) depicts a comprehensive analysis of the numerical assessment of curvature parameter γ with speed of tetra hybrid cross nanofluid (blood) classifying shear thinning/thickening flow. Giving increasing value of said parameter reacts with greater velocity of blood. There are several advantages of increased blood flow in arteries like improved delivery of oxygen and nutrients, improved waste removal, reduced risk of blood clots, better regulation of body temperature, and improved cardiovascular health; disadvantages include increased blood pressure, decreased efficiency of gas exchange, and reduced blood flow to certain areas and increased risk of injury.

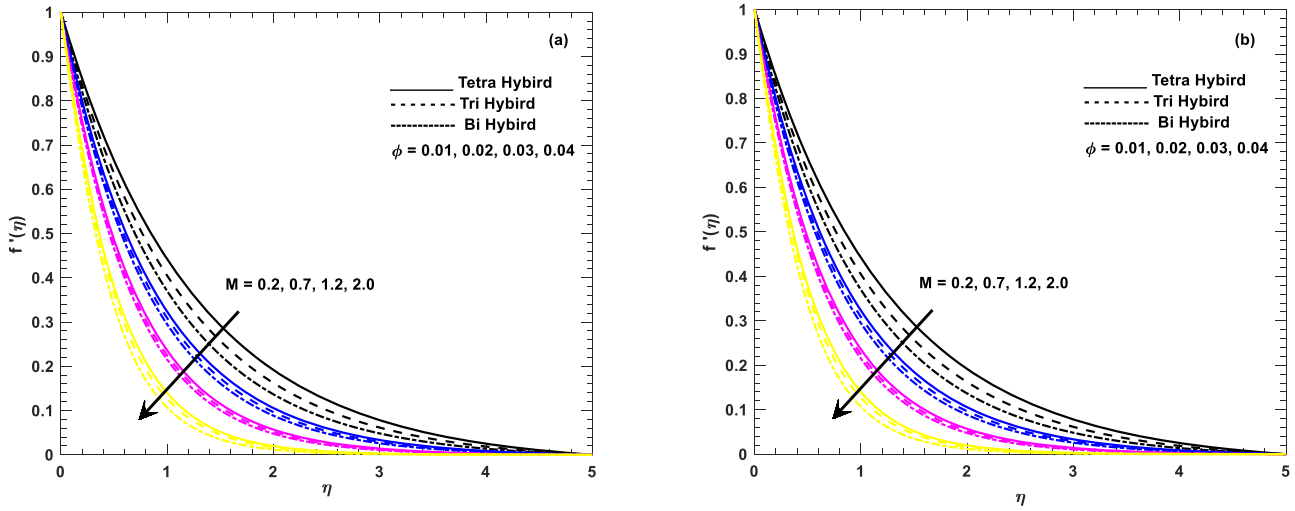

Figure 6: (a) and (b) Numerical assessment of M with speed of tetra hybrid cross nanofluid (blood) classifying shear thinning/thickening flow.

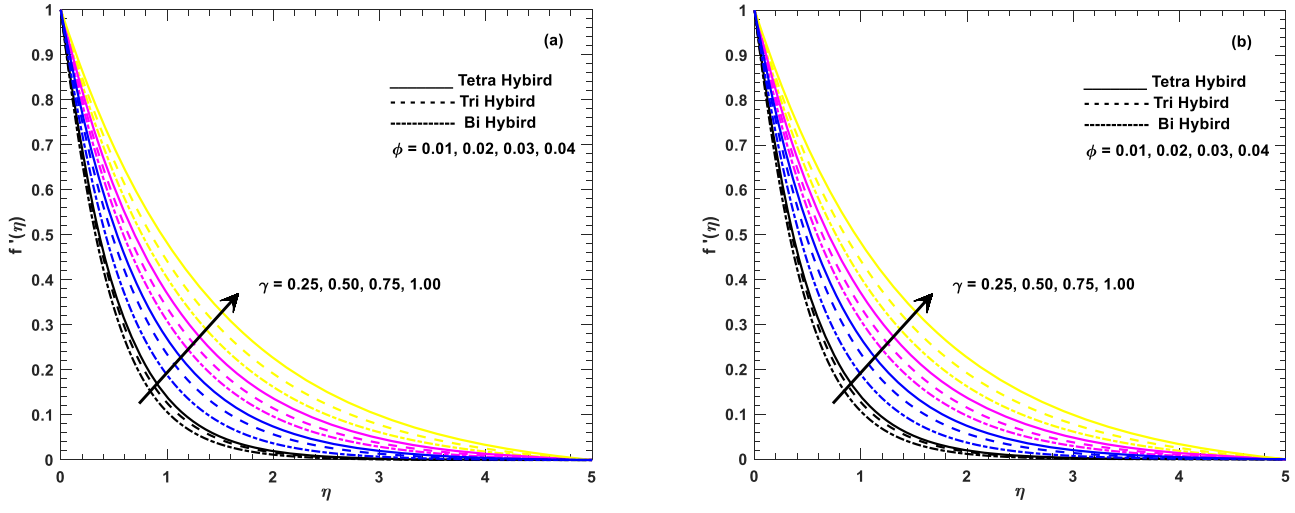

Figure 7: (a) and (b) Numerical assessment of γ with speed of tetra hybrid cross nanofluid (blood) classifying shear thinning/thickening flow.

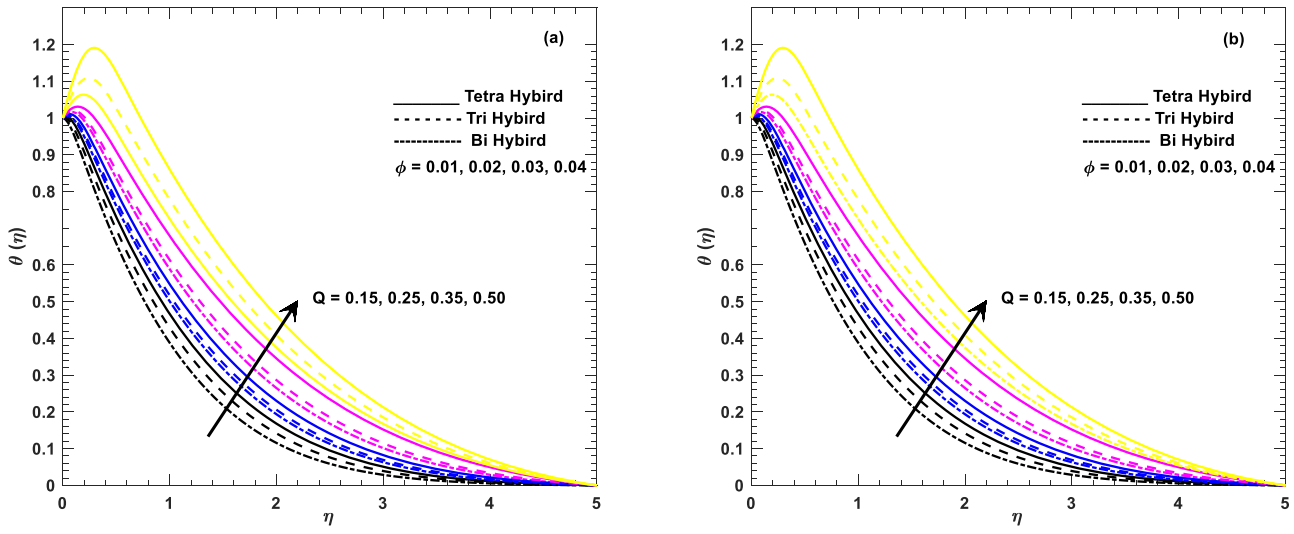

Figure 8: (a) and (b) Numerical assessment of Q with temperature of tetra hybrid cross nanofluid (blood) classifying shear thinning/thickening flow.

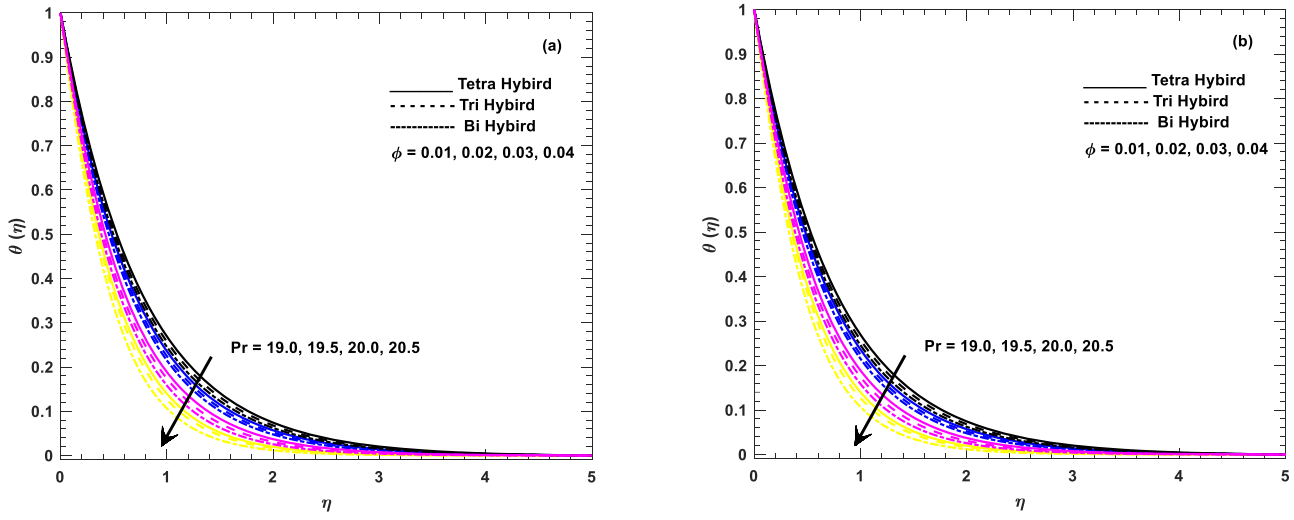

Figure 9: (a) and (b) Numerical assessment of Pr with temperature of tetra hybrid cross nanofluid (blood) classifying shear thinning/thickening flow.

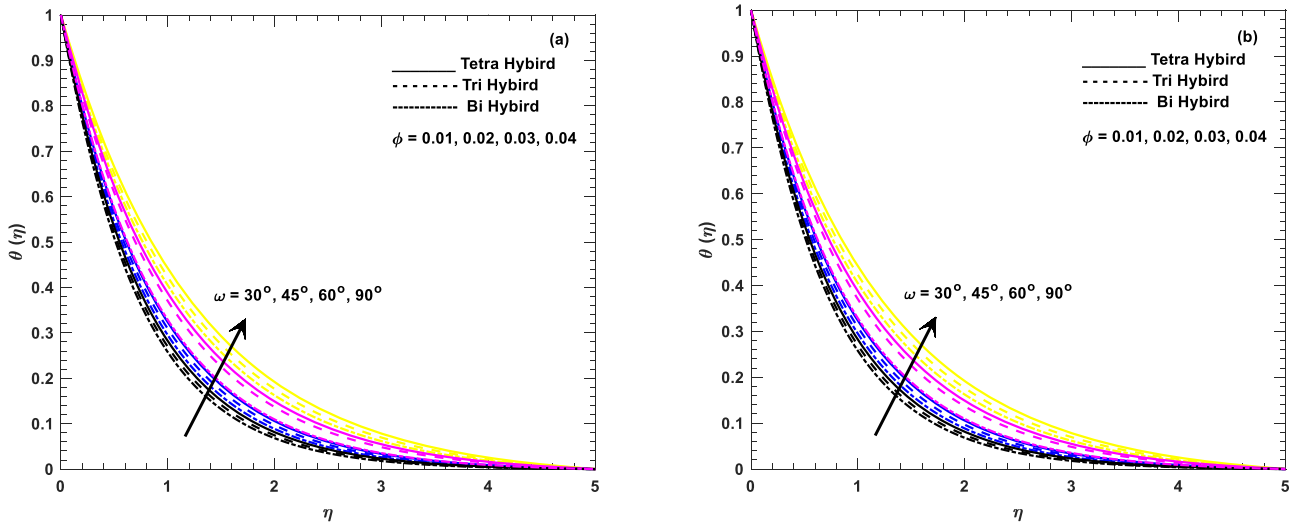

Figure 10: (a) and (b) Numerical assessment of ω with temperature of tetra hybrid cross nanofluid (blood) classifying shear thinning/thickening flow.

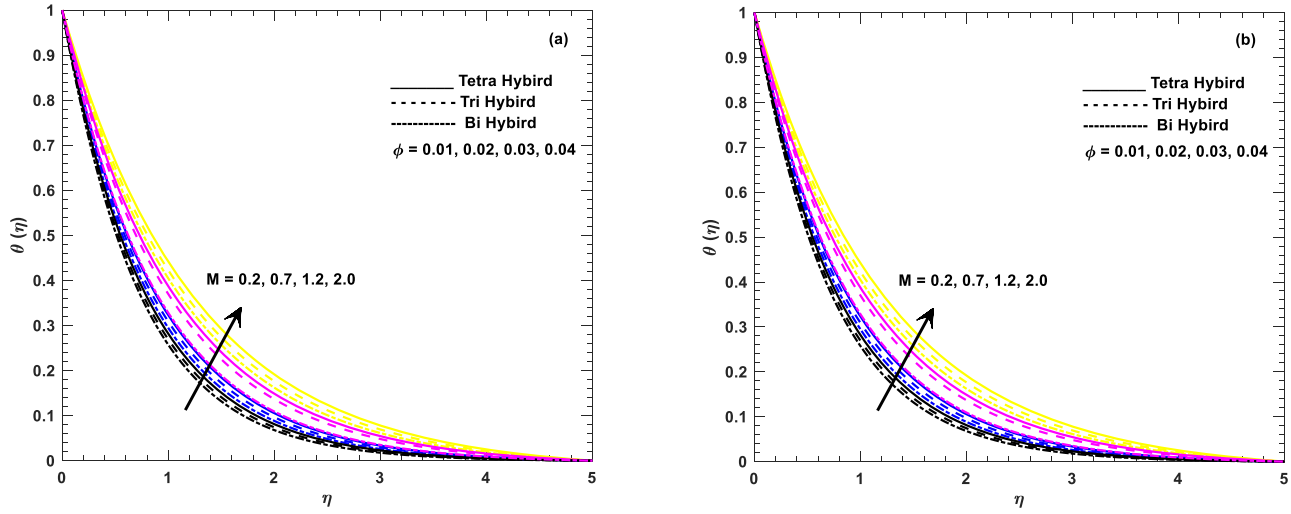

Figure 11: (a) and (b) Numerical assessment of *M* with temperature of tetra hybrid cross nanofluid (blood) classifying shear thinning/thickening flow.

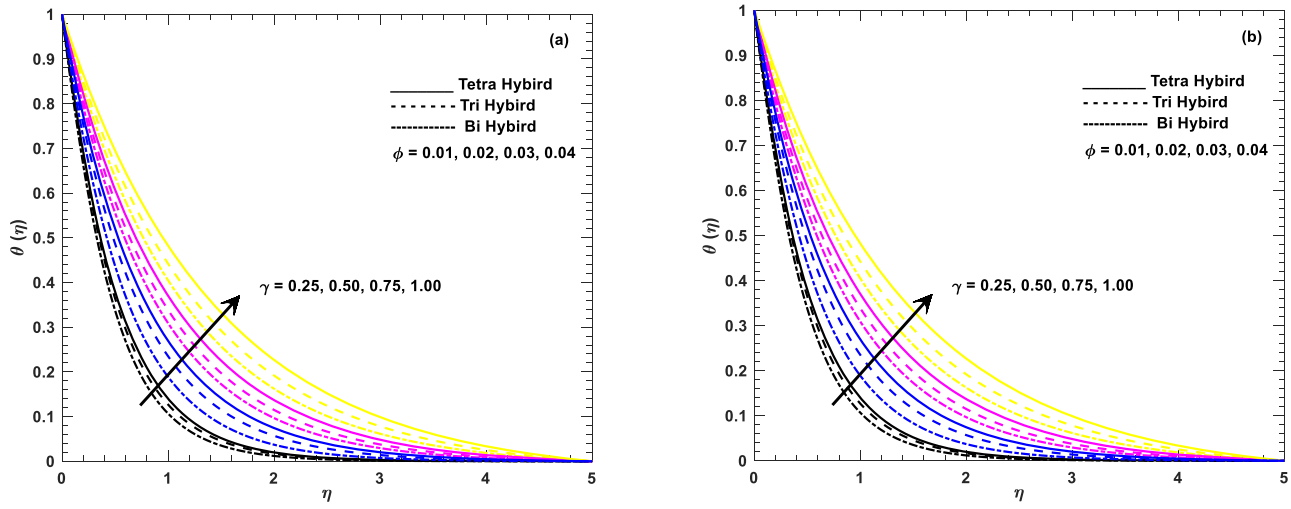

Figure 12: (a) and (b) Numerical assessment of *y* with temperature of tetra hybrid cross nanofluid (blood) classifying shear thinning/thickening flow.

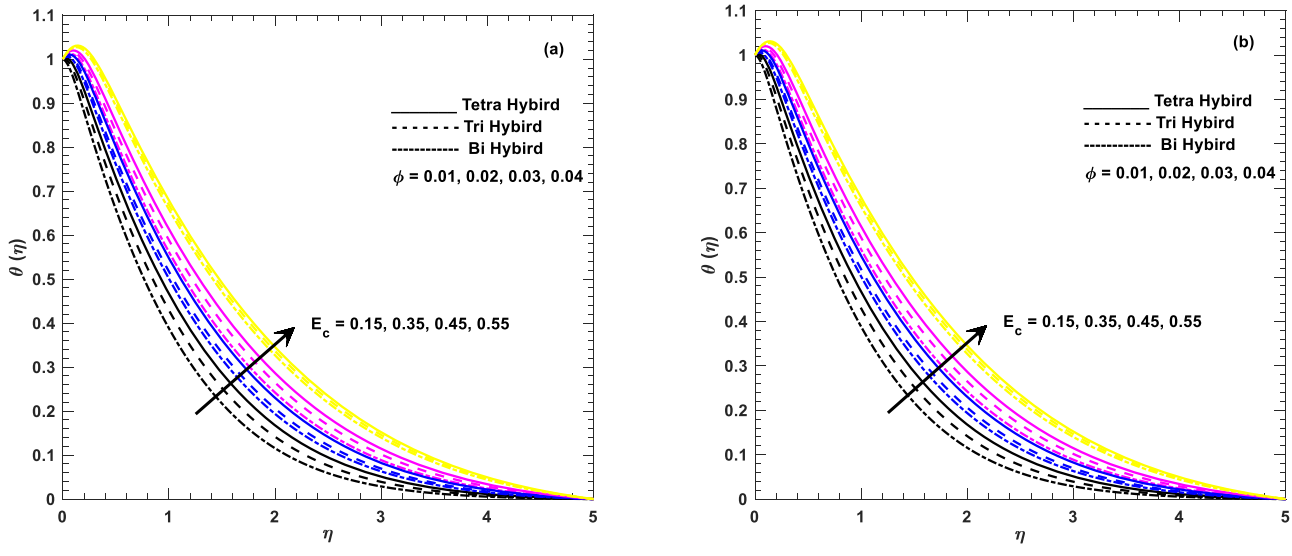

Figure 13: (a) and (b) Numerical assessment of E_c with temperature of tetra hybrid cross nanofluid (blood) classifying shear thinning/thickening flow.

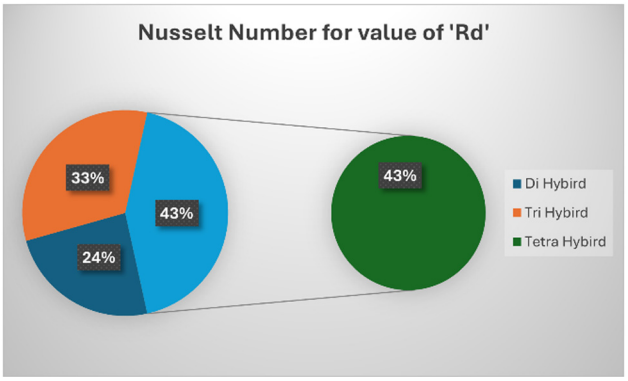

Figure 14: Statistical explanation of Nusselt number of tetra hybrid cross nanofluid (blood) with radiation parameter.

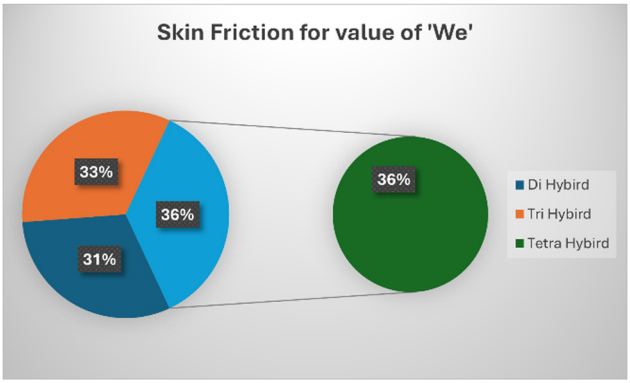

Figure 16: Statistical explanation of local skin friction of tetra hybrid cross nanofluid (blood) with We parameter.

Figure 8(a) and (b) are exercised to show the impact of Q with a temperature of tetra hybrid cross nanofluid (blood) classifying shear thinning/thickening flow. It is concluded that a greater value gives a higher temperature of the blood. Figure 9(a) and (b) is brought to show the impact of Pr with a temperature of tetra hybrid cross nanofluid (blood). Actually, the Prandtl number is not a property of blood itself, but still, it has an effect on the flow of blood in the body. The figure shows that with greater numerical input of this parameter, the temperature of blood decreases. Blood attached with a higher Prandtl number tends to have higher viscosity and lower rates of heat transfer. Blood has a relatively low Prandtl number compared to many other fluids. Figure 10(a) and (b) is launched to explore the numerical impact of the inclined angle of the magnetic field ω with temperature of tetra hybrid cross nanofluid (blood) (Figure 11). Greater value of the inclined angle the velocity decreases due to Lorentz force and hence temperature is increased. Figure 12(a) and (b) conclude that there is a direct impact of curvature parameter γ and temperature of tetra hybrid cross nanofluid (blood). Increasing the curvature parameter gives a higher temperature. Temperature becomes high with higher values of Ec. Frictional heating production is seen with this parameter. This fact is revealed by Figure 13(a) and (b). Physically, Ec represents difference in kinetic energy to the change in enthalpy that exists between both the wall as well fluid. Greater values of E_c turn kinetic energy into stored energy and fluid goes in viscous strains. The higher temperature has advantages and disadvantages for the body. Higher temperature is beneficial for enhanced metabolic activity, improved immune response, vasodilation, and improved cardiovascular function while other side effects are cellular damage, impaired blood clotting, dehydration, and worsened symptoms of certain medical conditions.

Numerical assessment of attached physical parameters on Local Nusselt Number and Local Skin Friction of Tetra hybrid/Tri Hybrid/Di Hybrid cross nanofluid (blood) classifying shear thinning/thickening flow and their pictorial representation is given by Figures 14–16.

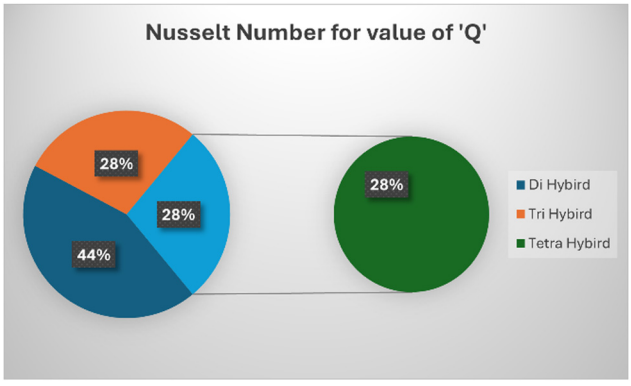

Figure 15: Statistical explanation of Nusselt number of tetra hybrid cross nanofluid (blood) with Q parameter.

7 Conclusions

This study offers a novel approach to modeling blood flow in a stenosed artery, which could have important implications for the diagnosis and treatment of cardiovascular disease. The findings highlight the importance of considering the effects of viscosity on blood flow and the potential benefits of using hybrid nanofluid models to better capture the complex behavior of blood flow in the body. Some concluding remarks of this study are given as follows:

1) Tetra hybrid nanofluid has great capability of heat transport due to the inclusion of three nanoparticles.

2) Greater numerical inputs in We give lower speed of blood in both cases of shear thinning/thickening flow and hence cause several problems like reduced delivery of oxygen and nutrients, increased risk of blood clots, *etc.*
3) Rapid heat transport is seen in the case of tetra-hybridity nanofluid as compared to tri-hybridity and di-hybrid nanofluid.
4) Strong Lorenz force is generated, and this Lorentz force causes reduction in the velocity of the blood.
5) It is found that surface drag friction becomes weakened by augmentation of Weissenberg quantity We.
6) Giving the increasing value of curvature parameter reacts greater velocity of blood. There are several advantages of increased blood flow in arteries like improved delivery of oxygen and nutrients.
7) Greater value of the inclined angle the velocity decreases due to Lorentz force and hence temperature is increased.

8 Limitations of the study

- Certain parameters in the study might be assumed or idealized, possibly neglecting variations and complexities present in actual stenosed arteries.
- The tetra hybrid cross nanofluid model may oversimplify blood flow through stenosed arteries, potentially missing nuances in real-world behavior.
- The study might not consider all external factors affecting blood flow, such as patient physiology differences, diverse stenosis types, or concurrent medical conditions.
- Numerical assessments of physical parameters might be limited to specific ranges and assumptions, potentially overlooking various scenarios or variations.
- Findings may lack generalizability to broader populations or specific clinical contexts.
- Availability of study-generated data sets might be restricted.

Acknowledgments: This work was supported by the Deanship of Scientific Research, Vice Presidency for Graduate Studies and Scientific Research, King Faisal University, Saudi Arabia [Grant No. KFU241693].

Funding information: This work was supported by the Deanship of Scientific Research, Vice Presidency for Graduate Studies and Scientific Research, King Faisal University, Saudi Arabia [Grant No. KFU241693].

Author contribution: All authors have accepted responsibility for the entire content of this manuscript and approved its submission.

Conflict of interest: The authors state no conflict of interest.

References

[1] Bhatti MM, Marín M, Zeeshan A, Ellahi R, Abdelsalam SI. Swimming of motile gyrotactic microorganisms and nanoparticles in blood flow through anisotropically tapered arteries. Front Phys. Apr 2020;8:95. doi: 10.3389/fphy.2020.00095.
[2] Lopes D, Puga H, Teixeira JC, Lima R. Blood flow simulations in patient-specific geometries of the carotid artery: A systematic review. J Biomech. Oct 2020;111:110019. doi: 10.1016/j.jbiomech.2020.110019.
[3] Ju L, Yang W, Lan IS, Marsden AL. Fluid-structure interaction modeling of blood flow in the pulmonary arteries using the unified continuum and variational multiscale formulation. Mech Res Commun. Jul 2020;107:103556. doi: 10.1016/j.mechrescom.2020.103556.
[4] Zhao YC, Vatankhah P, Goh T, Michelis R, Kyanian K, Zhang Y, et al. Hemodynamic analysis for stenosis microfluidic model of thrombosis with refined computational fluid dynamics simulation. Sci Rep. Mar 2021;11(1):6875. doi: 10.1038/s41598-021-86310-2.
[5] Akhtar S, McCash LB, Nadeem S, Saleem S, Issakhov A. Mechanics of non-Newtonian blood flow in an artery having multiple stenosis and electroosmotic effects. Sci Prog. Jul 2021;104(3):003685042110316. doi: 10.1177/00368504211031693.
[6] Das P, Sarifuddin S, Rana J, Mandal PK. Solute dispersion in transient Casson fluid flow through stenotic tube with exchange between phases. Phys Fluids. Jun 2021;33(6):061907. doi: 10.1063/5.0052770.
[7] Shahzad H, Wang X, Ghaffari A, Iqbal K, Hafeez MB, Krawczuk M, et al. Fluid structure interaction study of non-Newtonian Casson fluid in a bifurcated channel having stenosis with elastic walls. Sci Rep. Jul 2022;12(1):12219. doi: 10.1038/s41598-022-16213-3.
[8] Sharma BK, Sharma P, Mishra NK, Noeiaghdam S, Fernandez-Gamiz U. Bayesian regularization networks for micropolar ternary hybrid nanofluid flow of blood with homogeneous and heterogeneous reactions: Entropy generation optimization. Alex Eng J. 2023;77:127–48.
[9] Sharma M, Sharma BK, Khanduri U, Mishra NK, Noeiaghdam S, Fernandez-Gamiz U. Optimization of heat transfer nanofluid blood flow through a stenosed artery in the presence of Hall effect and hematocrit dependent viscosity. Case Stud Therm Eng. 2023;47:103075.
[10] Dharmaiah G, Prasad JR, Balamurugan KS, Nurhidayat I, Fernandez-Gamiz U, Noeiaghdam S. Performance of magnetic dipole contribution on ferromagnetic non-Newtonian radiative MHD blood flow: An application of biotechnology and medical sciences. Heliyon. 2023;9(2).
[11] Guled CN, Tawade JV, Kumam P, Noeiaghdam S, Maharudrappa I, Chithra SM, et al. The heat transfer effects of MHD slip flow with

suction and injection and radiation over a shrinking sheet by optimal homotopy analysis method. Results Eng. 2023;18:101173.
[12] Arulmozhi S, Sukkiramathi K, Santra SS, Edwan R, Fernandez-Gamiz U, Noeiaghdam S. Heat and mass transfer analysis of radiative and chemical reactive effects on MHD nanofluid over an infinite moving vertical plate. Results Eng. 2022;14:100394.
[13] Parida SK, Mishra S, Dash RK, Pattnaik PK, Khan MI, Chu YM, et al. Dynamics of dust particles in a conducting water-based kerosene nanomaterials: A computational approach. Int J Chem React Eng. 2021;19(8):787–97.
[14] Al-Kouz W, Owhaib W, Ayub A, Souayeh B, Hader M, Homod RZ, et al. Thermal proficiency of magnetized and radiative cross-ternary hybrid nanofluid flow induced by a vertical cylinder. Open Phys. 2024;22(1):20230197.
[15] Al-Rashed AAAA, Kalidasan K, Kolsi L, Velkennedy R, Aydi A, Hussein AK, et al. Mixed convection and entropy generation in a nanofluid filled cubical open cavity with a central isothermal block. Int J Mech Sci. 2018;135:362–75.
[16] Bakthavatchalam B, Habib K, Saidur R, Saha BB, Irshad K. Comprehensive study on nanofluid and ionanofluid for heat transfer enhancement: A review on current and future perspective. J Mol Liq. 2020;305(1):112787.
[17] Shulepova EV, Sheremet MA, Öztop HF, Abu-Hamdeh N. Mixed convection of Al2O3-H2O nanoliquid in a square chamber with complicated fin. Int J Mech Sci. 2020;165:105192.
[18] Selimefendigil F, Öztop HF. Thermal and phase change process in a branching T-channel under active magnetic field and two rotating inner cylinders: Analysis and predictions by radial basis neural networks. Int J Heat Mass Transf. 2023;217:124548. doi: 10.1016/j.ijheatmasstransfer.2023.124548.
[19] Selimefendigil F, El-Sinawi AH, Oztop HF. Optimization of bifurcating channel cooling system for double inclined conductive panel system under inclined magnetic field. Int J Therm Sci. 2023;191:108358. doi: 10.1016/j.ijthermalsci.2023.108358.
[20] Selimefendigil F, Öztop HF. Multijet impingement heat transfer under the combined effects of encapsulated-PCM and inclined magnetic field during nanoliquid convection. Int J Heat Mass Transf. 2023;203:123764. doi: 10.1016/j.ijheatmasstransfer.2022.123764.
[21] Acharya N. Magnetized hybrid nanofluid flow within a cube fitted with circular cylinder and its different thermal boundary conditions. J Magn Magn Mater. 2022;564(2):170167.
[22] Goswami KD, Chattopadhya A, Pandit SK, Sheremet MA. Transient thermogravitational convection for magneto hybrid nanofluid in a deep cavity with multiple isothermal source–sink pairs. Int J Therm Sci. 2022;173:107376.
[23] Souayeh B, Ali Abro K, Siyal A, Hdhiri N, Hammami F, Al-Shaeli M, et al. Role of copper and alumina for heat transfer in hybrid nanofluid by using Fourier sine transform. Sci Rep (Nat). 2022;12:11307. doi: 10.1038/s41598-022-14936-x.
[24] Chabani I, Mebarek-Oudina F, Vaidya H, Ismail AI. Numerical analysis of magnetic hybrid nano-fluid natural convective flow in an adjusted porous trapezoidal enclosure. J Magn Magn Mater. 2022;564(2):170142.
[25] Rudraiah N, Barron RM, Venkatachalappa M, Subbaraya CK. Effect of a magnetic field on free convection in a rectangular enclosure. Int J Eng Sci. 1995;33:1075–84.
[26] Souayeh B, Gnaneswara Reddy M, Sreenivasulu P, Poornima T, Alarifi IM. Comparative analysis on non-linear radiative heat transfer on MHD Casson nanofluid past a thin needle. J Mol Liq. 2019;284:163–74. doi: 10.1016/j.molliq.2019.03.151.
[27] Souayeh B. Simultaneous features of CC heat flux on dusty ternary nanofluid (graphene + tungsten oxide + zirconium oxide) through a magnetic field with slippery condition. Mathematics. 2023;11:554. doi: 10.3390/math11030554.
[28] Sheikholeslami M, Gorji-Bandpy M, Ganji PRDD, Soleimani S. Magnetohydrodynamic free convection of Al2O3-water nanofluid considering thermophoresis and Brownian motion effects. Comput Fluids. 2014;94:147–60.
[29] Ashorynejad HR, Hoseinpour B. Investigation of different nanofluids effect on entropy generation on natural convection in a porous cavity. Eu J Mech B Fluids. 2017;62:86–93.
[30] Acharya N. Magnetically driven MWCNT-Fe3O4-water hybrid nanofluidic transport through a micro-wavy channel: A novel MEMS design for drug delivery application. Mater Today Commun. 2024;38:107844. doi: 10.1016/j.mtcomm.2023.107844.
[31] Acharya N. Magnetized hybrid nanofluid flow within a cube fitted with circular cylinder and its different thermal boundary conditions. J Magn Magn Mater. 2022;564(Part 2):170167. doi: 10.1016/j.jmmm.2022.170167.
[32] Souayeh B. Thermal performance analysis of oriented MHD convective flow and entropy production of hybrid nanofluids in a cavity induced by semicircles at different radii ratios. Z Angew Math Mech. 2024;104(9):e202400015. doi: 10.1002/zamm.202400015.
[33] Algehyne EA, Ahammad NA, Elnair ME, Zidan M, Alhusayni YY, El-Bashir BO, et al. Enhancing heat transfer in blood hybrid nanofluid flow with Ag–TiO2 nanoparticles and electrical field in a tilted cylindrical w-shape stenosis artery: A finite difference approach. Symmetry. 2023;15(6):1242.
[34] Darvesh A, Sánchez-Chero M, Reyes Reyes CA, Céspedes PAS, Alvarez MT, Cárdenas MFU, et al. Mathematical analysis of bio-nanofluid flow over a nonlinear tapering artery with stenosis conditions using cross fluid viscosity model. BioNanoScience. 2023;13(4):2082–95.
[35] Khan SA, Yasmin S, Waqas H, Az-Zo'bi EA, Alhushaybari A, Akgül A, et al. Entropy optimized ferro-copper/blood based nanofluid flow between double stretchable disks: Application to brain dynamic. Alex Eng J. 2023;79:296–307.
[36] Tripathi J, Vasu B, Bég OA, Gorla RSR. Unsteady hybrid nanoparticle-mediated magneto-hemodynamics and heat transfer through an overlapped stenotic artery: Biomedical drug delivery simulation. Proc Inst Mech Eng, Part H: J Eng Med. 2021;235(10):1175–96.
[37] Das S, Pal TK, Jana RN, Giri B. Significance of Hall currents on hybrid nano-blood flow through an inclined artery having mild stenosis: homotopy perturbation approach. Microvascular Res. 2021;137:104192.
[38] Toghraie D, Esfahani NN, Zarringhalam M, Shirani N, Rostami S. Blood flow analysis inside different arteries using non-Newtonian Sisko model for application in biomedical engineering. Comput Methods Prog Biomed. 2020;190:105338.
[39] Sarwar L, Hussain, A. Flow characteristics of Au-blood nanofluid in stenotic artery. Int Commun Heat Mass Transf. 2021;127:105486.